13

Ray-based and Wavefront-based 3D Representations for Holographic Displays

Masahiro Yamaguchi and Koki Wakunami*
Global Scientific Information and Computing Center, Tokyo Institute of Technology, Japan

13.1 Introduction

A three-dimensional (3D) holography display is capable of reproducing extremely high-quality 3D images by wavefront reconstruction [1–3]. Conventional 3D displays are stereoscopic or multi-view, but more advanced displays based on light-field or light-ray reconstruction have also been investigated actively [4–6]. Then questions arise, what is the advantage of wavefront reconstruction? Is it possible to integrate light-ray-based and wavefront-based systems? This chapter addresses a technology that converts 3D data represented by light-rays into wavefront data and vice versa, and shows how to make use of the advantage of holographic displays. A method for calculating *computer generated holograms* (CGH), which was developed for this purpose, is introduced and experimental results are demonstrated.

13.2 Ray-based and Wavefront-based 3D Displays

Figure 13.1 shows the illustrations of ray-based and wavefront-based 3D displays. In ray-based 3D displays, the light-rays traveling in all directions are reproduced on the display surface in the same manner as those that were reflected or scattered by real objects. Therefore, an observer can see the 3D image as if they were real objects [7]. Integral photography is one of the

*Universal Communication Research Institute, Ultra-Realistic Video Systems Laboratory, National Institute of Information and Communications Technology, Japan

Multi-dimensional Imaging, First Edition. Edited by Bahram Javidi, Enrique Tajahuerce and Pedro Andrés.

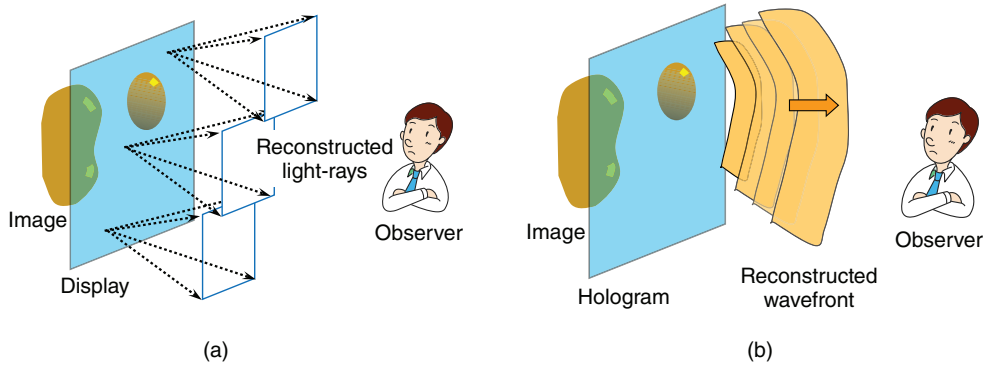

Figure 13.1 (a) Ray-based and (b) wavefront-based 3D displays

ray-based methods with both horizontal and vertical parallax (full-parallax: FP) information. Ray-based techniques have also been developed with *horizontal parallax only* (HPO). Contrary to multi-view or parallax-based methods, a method can be considered ray-based if more than one light ray is incident into the observer's eye pupil. In multi-view 3D displays, the discrepancy in depth perception by parallax and accommodation causes serious eye fatigue, but such discrepancies are diminished in ray-based techniques. In other words, the ray-based display enables 3D image formation by reproducing light rays.

Holography is a technique of wavefront recording and reconstruction as shown in Fig. 13.1(b). From the aspect of a 3D image display, it is important to understand the difference between ray-based and wavefront-based image reproduction. For this purpose, let us consider the wavefront reproduced by a ray-based display.

In references [8,9] the difference between a wavefront reproduced by a ray-based display and holography were discussed. Let us consider displays reproducing a point object as shown in Fig. 13.2. While a wavefront-based display reconstructs a spherical wave as in Fig. 13.2(a), a ray-based display generates an image of the point object by a set of converging rays as in Fig. 13.2(b). Every light ray emitted from a small area on the display plane can be considered a narrow plane wave propagating in different directions. Therefore, it can be said that two components are not reproduced by ray-based displays, whereas they are reproduced by holography; (1) the curvature of every small piece of plane waves, (2) the relative phase differences of the waves propagating in different directions. A component, the inclination of the wavefront depending on the relative location on the hologram plane with respect to the point object, is recorded in both displays.

Since those two components (1) and (2) are not managed in ray-based displays, the reconstructed point image will be broadened even if the sampling of light-rays is done at high density. This means the resolution of ray-based displays is limited compared with holography. It is possible to attach the relative phase difference component to the ray-based reproduction [9], which is called a *phase added stereogram* (PAS), if the optical path length of each light-ray is available. It has been shown that the resolution of the reconstructed image is improved by the PAS technique.

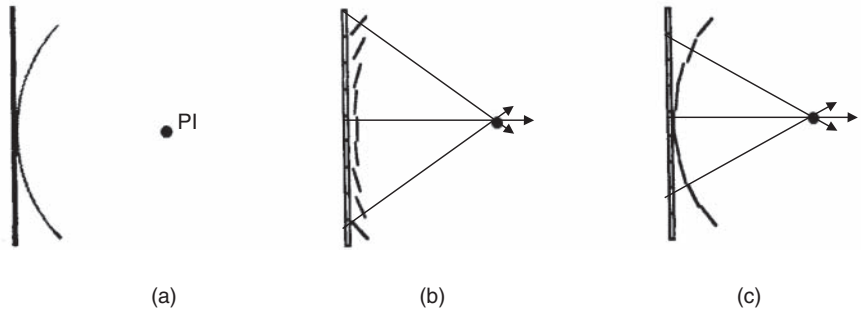

Figure 13.2 The wavefront reproductions by holographic, ray-based, and PAS-based displays for a *point image* (PI)

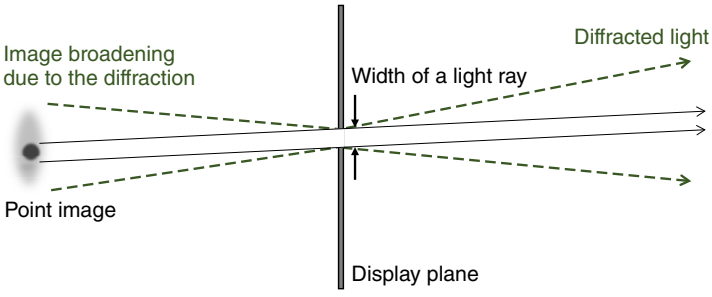

Figure 13.3 Image blur due to diffraction in ray-based displays

A PAS resembles a hologram. If the sampling density of light-rays is enough high, it becomes equivalent to a hologram. This means that ray-based reproductions can also be compared in the wavefront domain. In addition, the phase information of the reconstructed image is not important, but the resolution is the main issue in 3D display applications. Therefore, ray-based displays may be considered low level approximations of wavefront reconstruction, even though the previous two components are not included.

The difference in the wavefront shown in Fig. 13.2 causes a reduction in image resolution. Figure 13.3 shows the reconstruction of a single light-ray. The ray is diffracted on the display plane and the ray broadens at the image plane. If we consider the resolution of the reconstructed image, denoted by δ as the sum of the width of the light ray, d, and the diffraction effect, it is approximately written as

$$\delta = d + \frac{\lambda}{d}|z|, \tag{13.1}$$

where z is the distance of the point object from the display plane, and λ is the wavelength of the light, respectively. If the width of a light ray d expands, the diffraction effect decreases. However, the resolution becomes worse due to the width of the light lay. This is a fundamental

limitation of ray-based displays. The resolution can be kept high when z is small. Therefore the ray-based display is suitable for reproducing 3D images near the display plane.

Consider an observer with a visual acuity of 1.0 (in decimals or 20/20), located 500 mm away from the display: the observer can resolve 0.15 mm on the display plane. If we set $d = 0.15$ mm on the display plane, and let $\lambda = 0.5$ μm and $z = 200$ mm, the second term in Eq. (13.1) becomes 0.67 mm. The degradation in resolution is obviously perceivable by human vision. If we define the specification in the resolution of the reconstructed image as $\delta_l \geq \delta$, then the depth of the image that satisfies this condition is given by

$$|z| \leq \frac{d}{\lambda}\left(\delta_l - d\right), \tag{13.2}$$

and the right-hand side is maximized when $d = \delta_l/2$ and we have

$$|z| \leq \frac{\delta_l^2}{4\lambda}. \tag{13.3}$$

From this equation, when $\delta_l = 0.25$ mm, $|z| \leq 31$ mm; the image depth should be substantially smaller. For $\delta_l = 2$ mm, $|z| \leq 2000$ mm, which means that a ray-based display is suitable for larger sizes and lower resolution displays. As the resolution of the display is limited in ray-based methods, a holographic display is required especially when the display size is relatively small and/or the display is viewed close to the display plane.

According to the previous consideration, the main feature of a wavefront-based display is clarified: the reproduction of a deep 3D scene in high resolution, which is impossible with ray-based displays. A possible design for future holographic display is illustrated in Fig. 13.4 [10]. A very deep 3D scene is exhibited as a virtual window and the viewer can see the scene, not the display surface. It is expected that the technologies for holographic 3D displays will develop considering the application shown in Fig. 13.4.

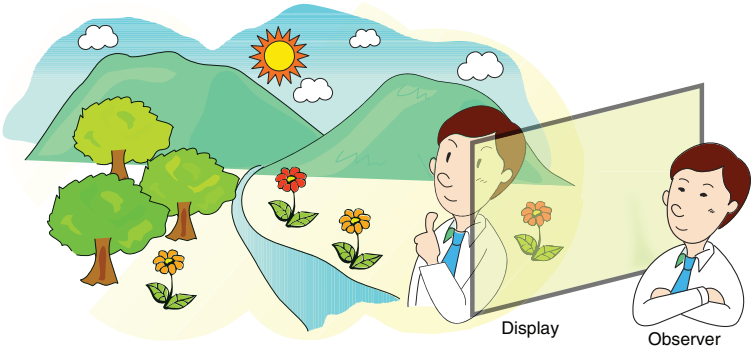

Figure 13.4 The concept of the display that can reproduce very deep and realistic 3D scenes

13.3 Conversion between Ray-based and Wavefront 3D Representations

To make use of the feature of wavefront-based display explained in Section 13.2, the wavefront on the hologram plane must be obtained. Various techniques for the computation of a hologram that simulates the wavefront propagation have been reported to date. However, for realistic display of 3D images, it is necessary to develop methods for representing various phenomena of light interactions. On the other hand, conventional rendering techniques for computer graphics are so advanced and extremely realistic representations are possible, such as occlusion, specular reflections, texture, translucency, and so on. Conventional rendering techniques for computer graphics are based on ray-tracing or light-fields. Thus the introduction of a ray-based rendering technique into wavefront-based displays will provide great benefits. Therefore, we developed a technique for conversion between ray-based and wavefront 3D representations, which enables the application of ray-based rendering techniques in the computation of holograms.

A light-ray represents the direction of energy flow, and is equivalent to a normal vector wavefront in an isotropic medium. Let us consider the wavefront in a small region on a certain plane in 3D space, as shown in Fig. 13.5, then its Fourier transform derives the angular spectrum. The spatial frequency of the angular spectrum corresponds to the direction of the wave propagation, which is parallel to the light ray that passes through the same region. Thus, the intensity of the angular spectrum is considered to be the intensity of light rays.

Under this principle, the conversion from a set of rays to a wavefront is realized in following way; (1) The set of rays, or the light field, like the one shown in Fig. 13.1(a) is sampled on a certain plane as depicted in Fig. 13.6. The plane for light-ray sampling here is called the *ray-sampling plane* (RS plane) [11]. The light-field can be generated by arbitrary rendering

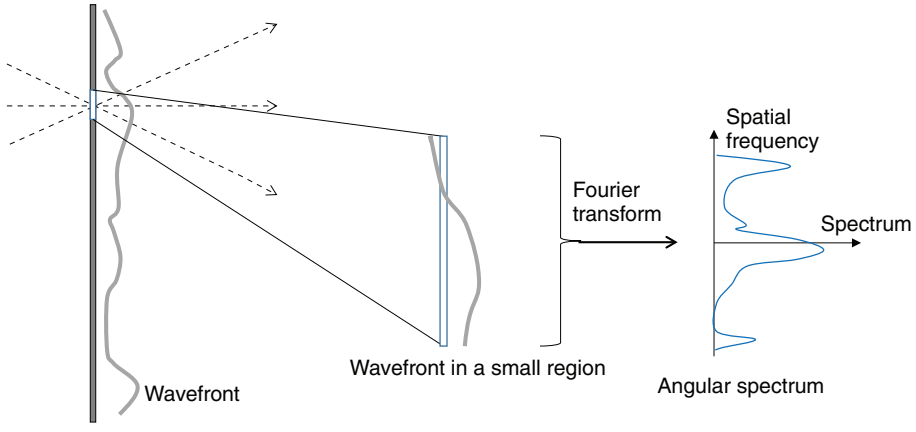

Figure 13.5 The relationship between the light-ray and the wavefront. If considering the wavefront in a small region on a certain plane, its Fourier transform gives the angular spectrum. The spatial frequency of the angular spectrum corresponds to the direction of wave propagation, and the intensity of a particular frequency is considered to be the intensity of the light-ray propagating in the corresponding direction

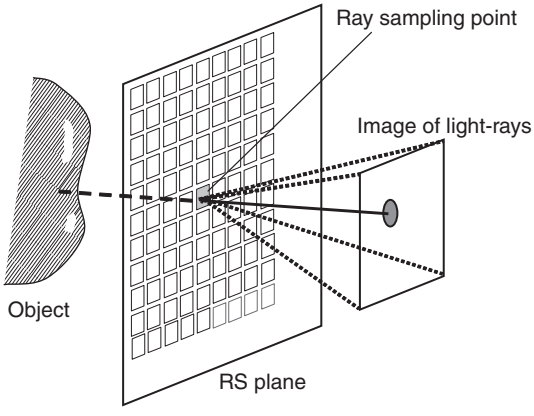

Figure 13.6 Sampling of light rays on the RS plane

techniques for computer graphics. (2) The image of rays that path through a point on the RS plane, which is an image of light rays indicated in Fig. 13.6, is Fourier transformed. Since phase information is not included in the light rays, the phase of each ray should be defined before the Fourier transform. It is possible to assign the phase on the basis of the theory of PAS explained in Section 13.2, or use of random or pseudo-random sequences are other options for phase distribution. If the rays are obtained by inverse conversion from wavefronts to rays, the phase information in the angular spectrum should be retained. The method for assigning phase information to light rays is an issue for further investigation. (3) The Fourier spectrum obtained by the second step is placed at the corresponding location on the RS plane. All the small blocks are converted in the same manner and then the wavefront on the RS plane is obtained.

13.4 Hologram Printer Based on a Full-Parallax Holographic Stereogram

13.4.1 Holographic 3D Printer

A holographic 3D printer was originally proposed on 1990 [7], in which the technique for automatic recording of a *FP holographic stereogram* (HS) was used. In FP-HS, the light ray's path through the hologram plane is recorded at high density; it then enables the observation of distortion-free 3D images from arbitrary locations within the viewing zone. HPO hologram printers have been studied since the 1990s [12–16], and the technology of FP-HS has also been commercialized [18]. The author's group has developed the technology for high-density recording of light rays, and achieved a spatial resolution 50–200 μm and angular resolution ≅ 0.3° in full-color FP-HS [18].

13.4.2 Full-Parallax Holographic Stereogram

In recording FP-HS, first a set of images for exposure is prepared using a graphics technique such as ray-tracing or *image-based rendering* (IBR) as shown in Fig. 13.6. The image of

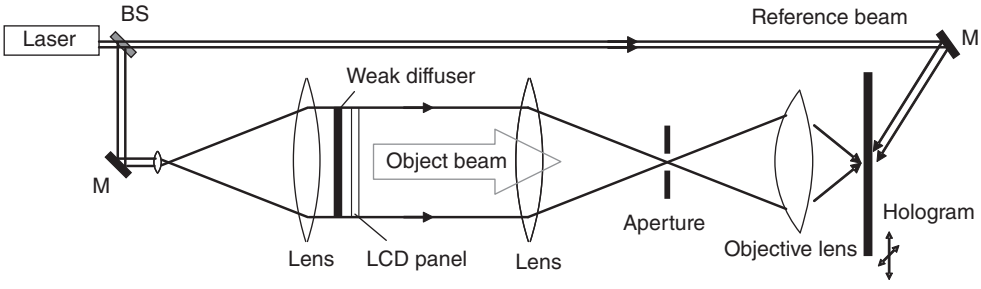

Figure 13.7 The optical system for FP-HS recording. BS: beam splitter, M: mirror, LCD: liquid crystal display. The hologram recording material is set to a XY translation stage to move horizontally and/or vertically after each exposure

light-rays for every block on the RS plane is used as the image for exposure by the optical system shown in Fig. 13.7. The image for exposure is displayed on a spatial light modulator such as liquid crystal display (LCD), which is illuminated by a plane wave from a laser light source, and an objective lens converts the plane wave to converging spherical wave. The holographic recording medium is placed at the focal plane of the objective lens, and the interference pattern with the reference beam that come from the opposite side is recorded in a small area. The small hologram is called elementary hologram (sometimes called a "hogel" [18]). A weak diffuser is used near the LCD panel to homogenize the intensity variation of object beam on the hologram plane [19]. After the exposure of an elementary hologram, the recording medium

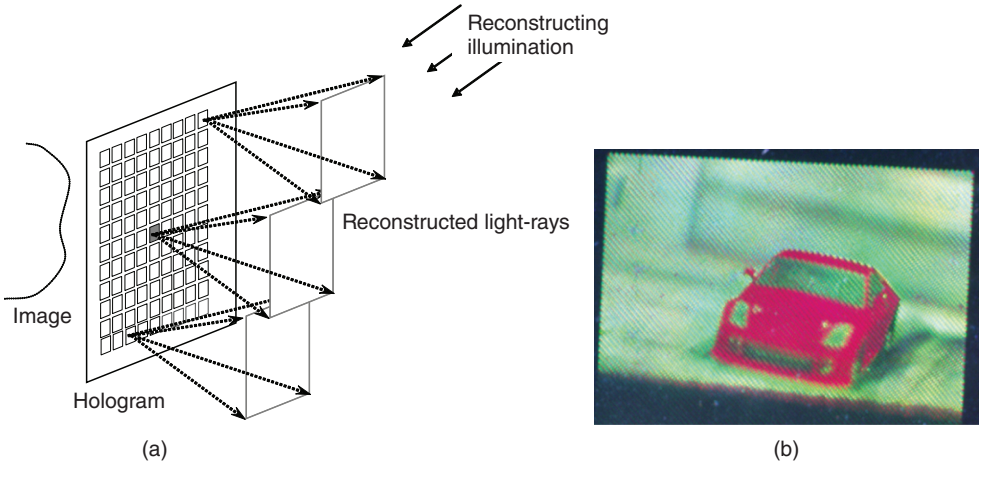

Figure 13.8 (Plate 22) Reconstruction of FP-HS. (a) Every elementary hologram reconstructs light rays in all directions. The light field is reproduced as all elementary holograms are illuminated simultaneously. (b) Example of the reconstructed image from full-color FP-HS hologram [20]. *Source*: T. Utsugi and M. Yamaguchi 2013. Reproduced with permission from The Optical Society. *See plate section for the color version*

is moved slightly in the horizontal/vertical direction for the next exposure. By exposing the whole hologram plane, FP-HS is obtained.

In the hologram printer system, a thick holographic medium is used and volume hologram is recorded. Then monochromatic image is reconstructed under white light illumination owing to the wavelength selectivity of the volume hologram. Using red, green, and blue lasers, full-color images have been also recorded. In the reconstruction of hologram, all elementary holograms simultaneously reproduce 2D images, as shown in Fig. 13.8(a). Each elementary hologram reproduces light rays traveling to different directions from the location of the grid point. Then the light field is reconstructed and a viewer can see the reproduced image as if there were real objects. Figure 13.8(b) (Plate 22) shows an example of the reconstructed image.

The optical arrangement shown in Fig. 13.7 is an optical Fourier transform system, and elementary holograms are the Fourier transform holograms of the image for exposure. This means that the wavefront reconstructed from FP-HS is a superposition of sets of wavefronts converted from light rays. Therefore this is a hologram but is also a ray-based 3D display. If the 3D image is located near the hologram plane, the difference between ray-based and wavefront displays can be kept small, and can be regarded an approximation of a real hologram. In such case, FP-HS can be considered as ray-to-wavefront converter.

13.5 Computational Holography Using a Ray-Sampling Plane

13.5.1 Computational Techniques for Electro-Holographic 3D Displays

The main purpose of the ray and wavefront conversion method is to apply it to the computation of holograms for electronic display. To realize electro-holographic 3D display in future, the technology for hologram computation is one of the principal issues as along with the ultra-high resolution display device. There have been various studies on this issue. A basic method for computing CGH is the superposition of spherical waves from a set of point light sources defined on the object surface [3,21]. It is called the *point-source method* (PSM) hereafter. In the PSM the light propagation is correctly simulated and hence high-resolution image can be reconstructed even when the image is distant from the hologram plane. A polygon-based method has also been proposed and the reproduction of excellent quality 3D images has been achieved [22].

Another approach for CGH has been also studied, which can utilize the techniques of conventional computer graphics. It is based on the principle of HS or light ray reproduction. Early work reported the CGH of HS [23], which corresponds to the multi-view 3D display. However, as the resolution of parallax views is increased, this can be deemed a light-field display. A set of parallax images is calculated using rendering technique of computer graphics, and taking the Fourier transform of each parallax image, the wavefront on the hologram plane can be derived as explained in Section 13.3. It is possible to obtain CGH of realistic 3D images by exploiting a variety of conventional rendering techniques. Nevertheless it should be noted that the image resolution is limited if the image location is distant from the hologram plane.

Since the important feature of holographic display is the capability to reproduce a deep 3D scene in high-resolution, both the methods explained earlier may not be satisfactory for this purpose. The method presented in the following sections [11] aims to take the merits of those wavefront-based and ray-based approaches.

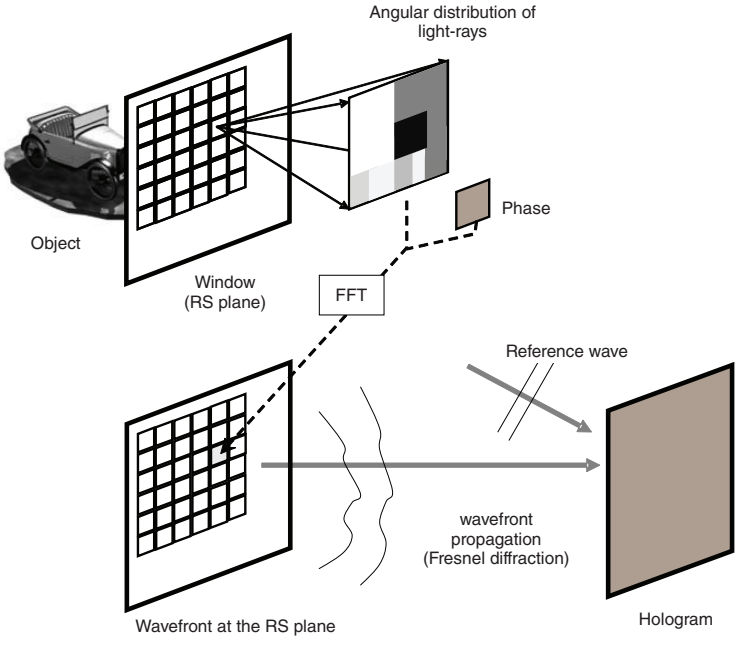

Figure 13.9 The schematic diagram of CGH calculation technique using the RS plane. In the upper figure, the angular distribution of light rays is collected at each sampled point on the RS plane. The ray information is Fourier-transformed after the random phase modulation, yielding the wavefront of a small area on the RS plane (lower figure). After all the ray information is transformed, the obtained wavefront is Fresnel-transformed to derive the wavefront on the hologram plane

13.5.2 Algorithm for CGH Calculation Using a Ray-Sampling Plane

In the proposed method for CGH calculation, a rectangular window is defined near the object location, and the images of light-rays are derived as already shown in Fig. 13.6, where the window is equivalent to the RS plane. As depicted in Fig. 13.9, the light field is sampled on the RS plane. However, the RS plane does not represent the hologram plane in contrast to Section 13.4. Now we intend to reproduce a deep 3D scene. By locating the RS plane near the object, the degradation due to ray sampling and the diffraction effect can be kept satisfactory small, and it is possible to avoid degradation of resolution. The conversion from the light field to wavefront described in Section 13.3 is applied on the RS plane; taking the Fourier transform of the angular distribution of light-ray intensity, after a random phase pattern is attached to the image so as to homogenize the intensity variation on the RS plane. Then the wavefront on the RS plane is obtained. Next, the wavefront propagation from the RS plane to the final hologram is simulated by Fresnel transform and the hologram fringe is obtained by the interference with a reference wave.

The features of the proposed method are summarized as follows:

- High-resolution sampling is possible even for the objects distant from the display plane, since light rays are sampled near the objects.

- Image blur or artifacts due to diffraction do not affect the reconstructed image because the propagation from the RS plane to the hologram is calculated based on diffraction theory.
- If the RS plane is defined in parallel to the hologram plane, the distance of wave propagation is constant, and high-speed computation of Fresnel diffraction can be implemented by using FFT (*Fast Fourier Transform*).

13.5.3 Comparison with Ray-based Techniques

First the reconstructed image of the proposed method (RS) was compared with that of the ray-based method (R-CGH hereafter) by numerical simulation [11]. In this case a 2D object was defined and located 10 and 200 mm behind the hologram plane as shown in Fig. 13.10. In the proposed method, RS plane is defined at 5 mm front of each object plane, while in R-CGH the rays are sampled at the CGH plane. The number of sampling points is 128 × 128, the number of angular sampling was 32 × 32 in both R-CGH and proposed method, and the total number of pixels of CGH was 4096 × 4096. To simulate reconstruction, an imaging lens with a 7 mm pupil size that mimics the human eye was defined and the reconstructed image calculated by scalar diffraction theory.

Figure 13.11 shows the simulated reconstructed images. It can be confirmed that a high-resolution image was reproduced by the proposed method, while the image reconstructed by ray-based hologram was blurred to large extent.

13.5.4 Optical Reconstruction

In the experiment, a CGH was calculated by the proposed technique and recorded in a holographic recording material using a CGH printer developed for this purpose [11]. For the object shown in Fig. 13.12(a), a car, the images of various different views were calculated by using an off-the-shelf rendering software. Then the images of angular ray-distribution were calculated based on the IBR technique. The object is located 200 mm behind the hologram plane and the image size was about 50 × 50 mm. The number of ray-sampling points was 768 × 768, the size of a ray-sampling point was 64 × 64 μm, and the number of rays in each ray-sampling point was 32 × 32. The total number of pixels of the CGH was 24 576 × 24 576 pixels. The

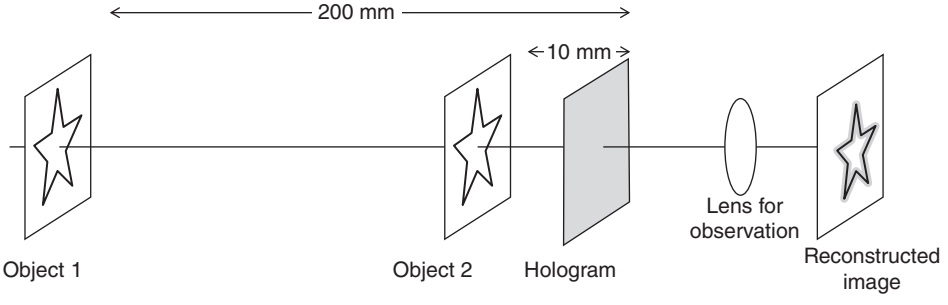

Figure 13.10 Geometry for simulation

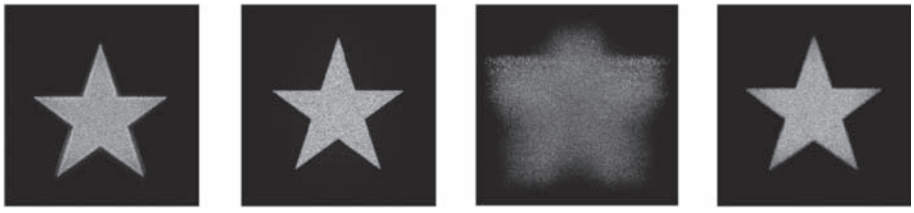

Figure 13.11 Simulation result. Reconstructed images of object 2 by (a) R-CGH and (b) proposed method. Reconstructed images of object 1 by (c) R-CGH and (d) proposed method. The object and hologram are both in 8×8 mm

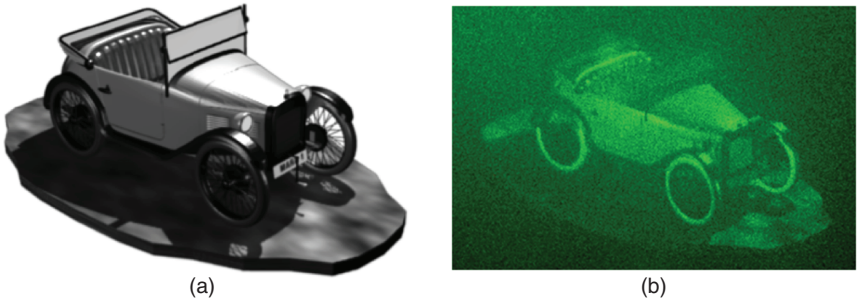

Figure 13.12 (a) The object rendered by computer graphics software. (b) Optical reconstruction of the CGH generated by proposed computation technique using the RS plane

calculated CGH pattern was exposed onto a holographic recording material using the fringe printer described previously. The image reconstructed by a plane wave generated from a DPSS (*Diode-Pumped Solid State*) green laser of 532 nm is shown in Fig. 13.12(b). As the pixel pitch of the recorded CGH was about 2 μm, the viewing angle is limited in ±3.6°. It can be observed that the surface reflection property is exhibited by rendering graphics.

13.6 Occlusion Culling for Computational Holography Using the Ray-Sampling Plane

13.6.1 Algorithm for Occlusion Culling Using the Ray-Sampling Plane

Occlusion processing is one of the important issues in the calculation of holograms [22,24–26]. In ray-based rendering, the hidden surface removal can be done by a z-buffer or ray-tracing. However, occlusion culling has not been established in the simulation of wave propagation. Strictly speaking, the wave equation should be solved with boundary conditions given by the object arrangement, but it is not practical because computation becomes very complicated. A method for exact occlusion culling was reported in [25] where the wave propagation was calculated step-by-step for every depth where occlusion took place. But

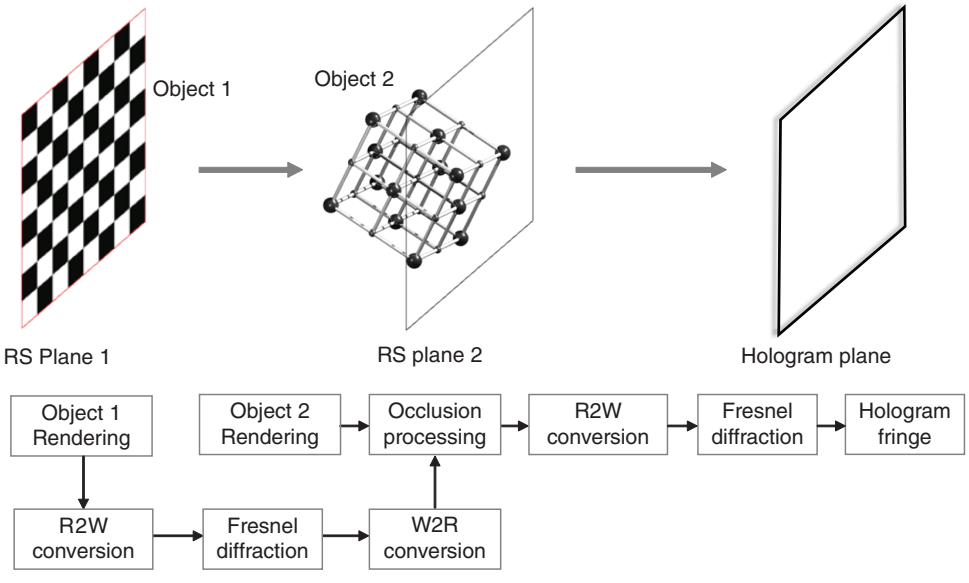

Figure 13.13 Schematic diagram of the proposed method incorporating mutual occlusion processing. R2W and W2R represent ray-to-wavefront and wavefront-to-ray transformations, respectively

such a method requires a lot of computation and most of the previous work on occlusion processing was based on ray tracing. In reference [25], the wavefront from the hidden surface was removed on the hologram plane. In this case, the diffraction of the light emitted from the hologram was taken into account, but the diffraction by the interrupting object was not. If the hologram reconstructs a very deep scene, the diffraction by the interrupting object cannot be ignored. A simple method for this purpose, called the silhouette method, was also proposed, in which the occlusion mask was defined near the interrupting object [22]. Although the calculation is simple, some errors can appear due to the discrepancy between depths of the interrupting object and the silhouette mask.

In the proposed method using the RS plane, self-occlusion, some surfaces are hidden by other surfaces of the same object, and this can be directly achieved by the rendering technique. Another type of occlusion, mutual occlusion between different objects, should be dealt with by defining an RS plane for each object located at different depths, as shown in Fig. 13.13. In the occlusion culling method using the RS plane [26], the conversion from wavefront to ray, as well as the conversion from ray to wavefront, is employed as follows.

The wavefront propagation from the RS plane 1 to the RS plane 2 is first calculated by Fresnel transformation to derive the wavefront on the RS plane 2, and is converted to the ray-information using inverse Fourier transform (W2R) on the second RS plane. Then occlusion processing is realized in the light-ray domain; the rays from the RS plane 1 are overwritten by those from the object 2. If there is no ray from object 2 at a certain location on the RS plane 2 traveling to a certain direction, then the ray from the background object is used. The

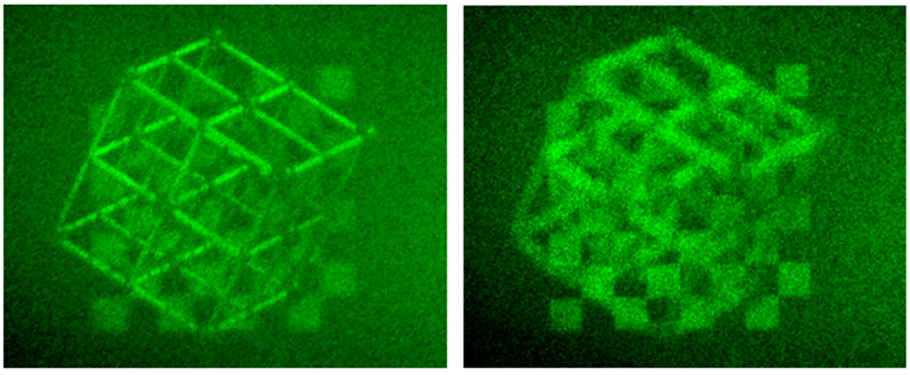

Figure 13.14 Results of optical reconstruction of the hologram calculated by the proposed method. The camera focus was adjusted to the front object in the left and the background object in the right

ray-information after occlusion processing is converted to wavefront (R2W) again, and the Fresnel transformation gives the wavefront on the hologram plane.

13.6.2 Experiment on Occlusion Culling Using the Ray-Sampling Plane

To prove the capability of occlusion culling using the RS plane, an experiment was carried out. Two objects, front and background as shown in Fig. 13.13, were used in this experiment. RS planes were defined at 100 and 150 mm behind the hologram plane, the background object was located on the RS plane. The hologram size and resolution were 50×50 mm and $16\,384 \times 16\,384$ pixels, respectively. Figure 13.14 shows the reconstructed images with changing the focusing position. Both the self and mutual occlusions were represented correctly and focusing on each object was possible.

13.7 Scanning Vertical Camera Array for Computational Holography

13.7.1 Acquisition of a High-Density Light Field

The holographic 3D printer introduced in Section 13.4 and the CGH using RS plane presented in Sections 13.5 and 13.6 are both generated from the ray-based 3D data. The images presented in Fig. 13.14 were synthesized by artificial computer graphics but it is also expected they can produce holograms of real pictured objects. In the HPO case, shooting images for HPO 3D is not as difficult as using horizontal camera motion or a horizontal camera array. On the other hand, capturing FP images requires much effort, and large-scale systems that use a huge number of cameras have been reported for light-field acquisition [3,27,28]. It is also possible to apply model-based rendering using 3D measurement and texture mapping, but the reproduction of high-fidelity realistic images, capturing and modeling of angular dependent reflections have turned out to be complicated, and the problems due to occlusion often affect

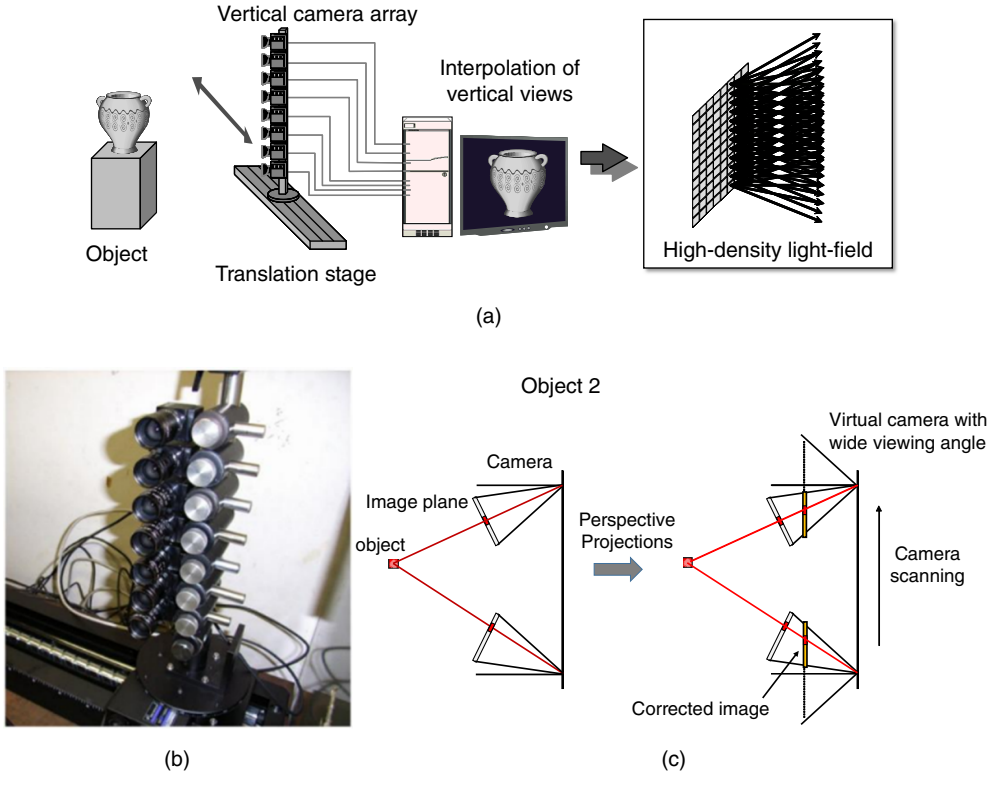

Figure 13.15 (a) Scanning vertical camera array system for the acquisition of high-density light field information. (b) Experimental of vertical camera array. (c) Geometry for keystone distortion correction

3D images as well. In this chapter, a relatively simple system for capturing the FP light field of still images is presented with a scanning vertical camera array [29].

13.7.2 Scanning Vertical Camera Array

In the proposed system, a vertical camera array is scanned horizontally as shown in Fig. 13.15(a), and vertical parallax information is interpolated from the captured data. Then only a small number of cameras are required, which allows relatively simple and compact implementation. Figure 13.15(b) shows the vertical array of seven cameras controlled by a single PC, which was used in the following experiment.

If light-rays are captured by horizontal scanning of a camera array, the angular range of rays is limited by the angle of view of the camera. In order to acquire wider angular range, the camera array is rotated with the horizontal motion such that the camera is always pointed at the object as shown in Fig. 13.15(c). In this converged camera motion, the captured images have keystone distortion. For the distortion correction, the image of a checkerboard pattern was captured in the experiment, and the parameters of keystone distortion were obtained in

advance. Then perspective projection was applied to derive the images that were virtually captured by the cameras arranged parallel to the camera motion axis. Figure 13.15(c) shows the keystone distortion correction. The distortion correction had been done in advance of the following steps.

13.7.3 Vertical Interpolation

To obtain high-density light-ray information, the rays passing through the gap between cameras are interpolated. In the system shown in Fig. 13.15(a), since the horizontal parallax information is captured at high-resolution, the depth of an object can be estimated at each pixel without much difficulty. With the depth information at each pixel, vertical views between cameras are interpolated by a *depth image-based rendering* (DIBR) technique [30].

The depth data are calculated for every pixel of captured images after the distortion correction. Stereo matching or *epipolar plane image* (EPI) analysis for depth estimation is first applied in the horizontal direction for this purpose. In horizontal matching, only a limited range of camera positions around the target camera is used as shown in Fig. 13.16(a). This is for the purpose to avoid mismatching due to possible object motion or specular reflection on the object surface because their effect increases if a long sequence of horizontal camera motion is used. But when the range of camera positions used in matching is small, the depth resolution becomes low. Therefore, from horizontal camera motion, the depth of each pixel is roughly estimated. Then another stereo matching is performed using the images captured by the cameras at different heights, for fine estimation.

The vertical interpolation is performed basing on the geometry shown in Fig. 13.16(b). Consider the interpolation between upper (camera 1) and lower (camera 2) cameras. The distance between lower and upper cameras is Δy in the vertical direction, and the height of the new

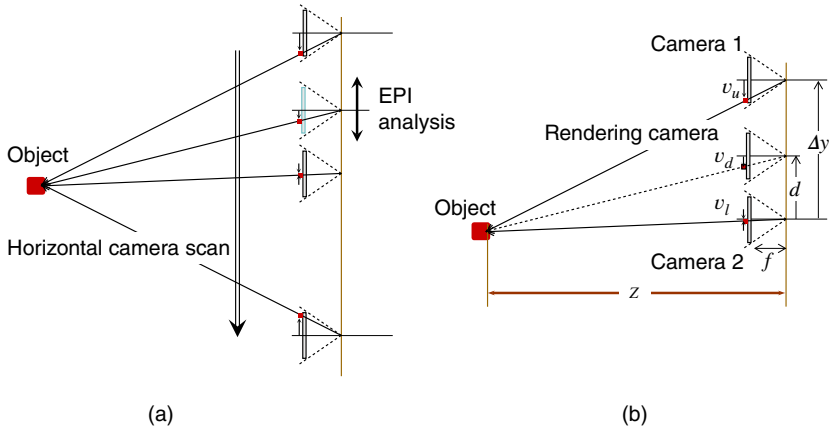

Figure 13.16 The geometry for depth estimation and vertical-parallax interpolation. (a) *Top view*: After the distortion correction, virtual cameras with wide viewing fields are moved in the horizontal direction. (b) *Side view*. The image of the rendering camera (new camera) is interpolated from the images captured by the upper (camera 1) and lower (camera 2) cameras

camera to be interpolated is d from the lower camera. f denotes the distance between the image plane and the projection center.

Let the depth of a point photographed at v_u on the upper camera image be z, then the same point should be projected at v_l in the lower camera image, given by

$$v_l = v_u + \frac{f}{z}\Delta y, \tag{13.4}$$

if occlusion does not affect the corresponding point. So, the estimated depth of the pixel at v_l of lower camera image should be almost equal to that of the pixel at v_u of upper camera image. Then, in the image of a new camera, $f_d(u, v)$, the pixel value is given by the linear interpolation of upper and lower images as,

$$f_d\left(u, v_u + \frac{f}{z}d\right) = \frac{d}{\Delta y} f_u(u, v_u) + \left(1 - \frac{d}{\Delta y}\right) f_l\left(u, v_u + \frac{f}{z}\Delta y\right), \tag{13.5}$$

where $f_l(u, v)$ and $f_u(u, v)$ denote the pixel values of lower and upper camera image, respectively. If no corresponding points are found in a vertical camera pair, the interpolation using either upper or lower images is applied, or the result of horizontal matching is used.

13.7.4 Synthesis of Ray Images

Next, the light-ray images are synthesized from a set of interpolated camera images. Figure 13.17 shows the geometry for generating the ray image at kp_e of the RS plane, where $k = 0, 1, \ldots K-1$, K (is the number of RS points in horizontal dimension) is the index for

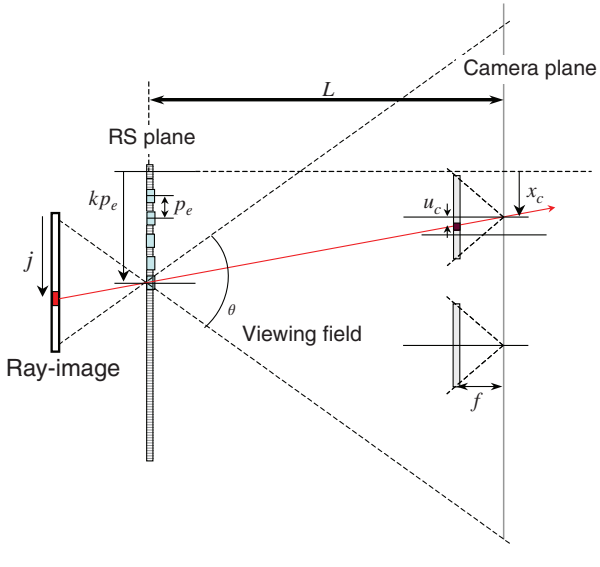

Figure 13.17 Synthesizing the ray image on the RS plane

a RS point and p_e is the sampling pitch of light rays on the RS plane. Only the example of horizontal direction is shown, where the same process is applied to both horizontal and vertical directions after the previous vertical interpolation.

The j-th pixel of the ray-image is picked-up from the image of the camera at x_c, as

$$x_c = kp_e - \left(\frac{j}{N-1} - \frac{1}{2}\right) 2L \tan\frac{\theta}{2}, \tag{13.6}$$

where $j = 0, 1, \quad \ldots \quad N-1, N$ is the number of pixels of the ray-image in horizontal dimension, L is the distance of the camera plane from the RS plane, and θ denotes the angle of viewing field. The location of the pixel in this camera image, u_c, is given by

$$u_c = -\left(\frac{j}{N-1} - \frac{1}{2}\right) 2f \tan\frac{\theta}{2}. \tag{13.7}$$

then the corresponding pixel can be found from the camera images. f is a parameter that determines the magnification of the camera image.

A set of the ray images is generated by the earlier image transform process, which is based on IBR. Note that the position of the RS plane should be set near the object, as discussed in Section 13.5, so as to avoid reducing resolution far from the RS plane.

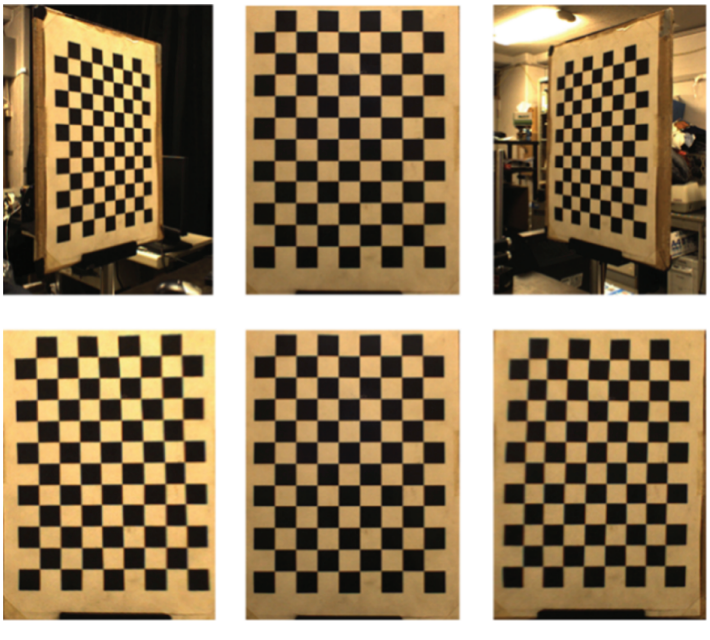

Figure 13.18 The results of distortion correction. *Upper row*: captured images, *Lower row*: corrected images corresponding to upper images

13.7.5 Experiment on Full-Parallax Image Generation

In the experiment, a FP 3D image captured by the proposed system was employed to synthesize holographic 3D images. The experimental system consists of seven compact CCD cameras (480 × 640 pixels, Point Gray Research, Flea) (see Fig. 13.15b) connected to PC through IEEE1394 interface, and a translation stage (Sigma, SGSP601200 (X)), which is also controlled by the same PC. The vertical intervals of cameras are 60 mm. The system is rather simple and concise, for a single PC can control the entire system. Scanning 576 mm in the horizontal direction and 577 × 7 images were captured in the experiment in 40 s, where the maximum angle of camera rotation was about 60°. The distortion correction described in Section 13.7.2 was applied as shown in Fig. 13.18.

Figure 13.19 Examples of camera images after distortion correction. Captured from (a) left, (b) center, (c) right, and (d) upper center

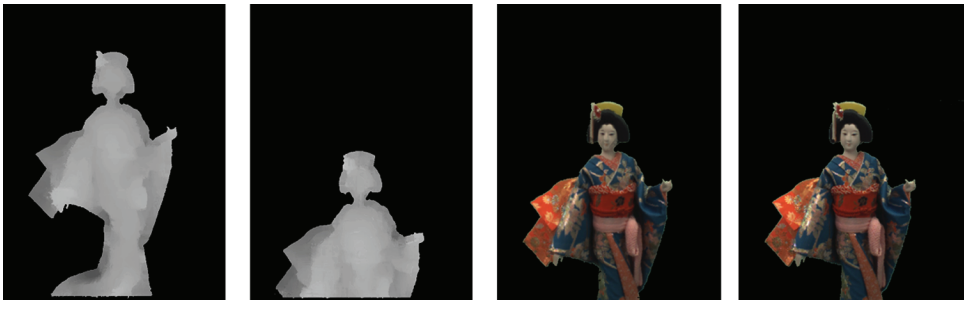

Figure 13.20 Estimated depth images for (a) Figure 13.19(b) and (b) Figure 13.19(d). (c) The result of vertical interpolation. (d) The image captured by real camera at the position of interpolated camera of (c)

The captured images after the distortion correction are shown in Fig. 13.19. Depth estimation was done by stereo matching analysis between the images of camera intervals at 6 mm, following stereo matching using a vertical camera pair. Block matching using SAD (*Sum of Absolute Difference*) with 25×25 pixel windows was used. In vertical matching the search area was only ± 5 pixels around the pixel estimated by horizontal matching. The estimated depth images are shown in Fig. 13.20(a) and (b). Figure 13.20(c) shows the interpolated image, where Fig. 13.20(d) represents the image captured by the real camera placed in the same position. The accuracy of the interpolated image was satisfactorily high, since both horizontal and vertical parallax information were effectively employed. The PSNR (*Peak Signal-to-Noise Ratio*) of the interpolated image was 28.64 dB, whereas it was 27.05 dB in the case when only vertical stereo matching was used and 27.16 dB for horizontal EPI analysis only; about 1.5–1.6 dB improvement was achieved.

The total number of interpolated images was 577 (H) $\times$ 361 (V) at 1 mm intervals. It is possible to generate free-viewpoint images using the light-field data acquired by the proposed system, though this is limited to still image applications. Figure 13.21 shows three different view images generated using the IBR technique. Excellent quality images were synthesized from high-density light-field data captured by the scanning system. It should be noted that the specular reflections are also well reproduced, which considerably contributes to the realism of the images.

In the next experiment, CGHs were recorded using the captured light-field data. An RS plane was defined near the object, and the CGH plane was defined about 200 mm apart from the RS plane (Fig. 13.22a). The number of RS points was 256×256 and the resolution of each ray-image was 64×64 pixels. The total number of pixels in RS plane and CGH was both $16\,384 \times 16\,384$ pixels. The sampling intervals and the sizes of RS plane and CGH were the same; 2.1 μm and 34.4×34.4 mm, respectively. The calculated CGH pattern was conveyed to the output using the CGH printer presented in Section 13.5. The images reconstructed by the 532 nm green laser are shown in Fig. 13.22(b) and (c). It can be confirmed that the images are fairly reproduced by CGH, although the quality is limited because the hologram size is small and the resolution of the CGH printer is not high enough.

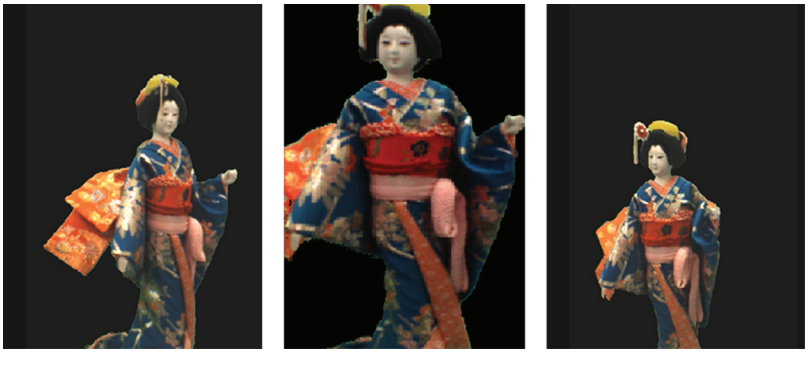

Figure 13.21 Free-viewpoint images generated from the light-field data captured by the proposed system. Left, close center, and upper right views

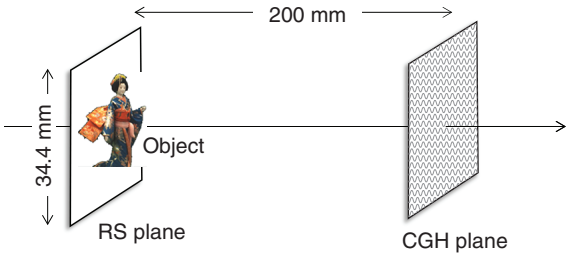

(a)

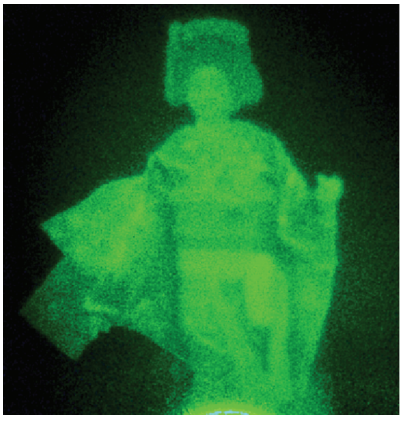

(b)

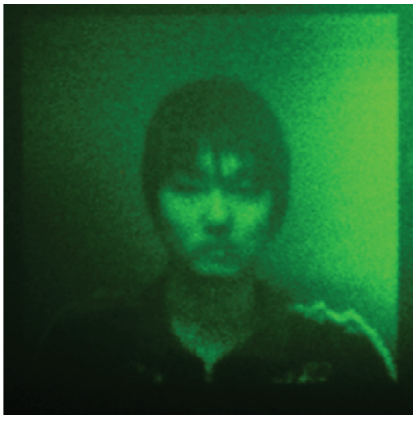

(c)

Figure 13.22 (a) The geometry for CGH calculation. The sizes of RS plane and CGH plane were both 34.4 mm. (b, c) Reconstructed images of the CGH. (b) Japanese doll, and (c) human portrait

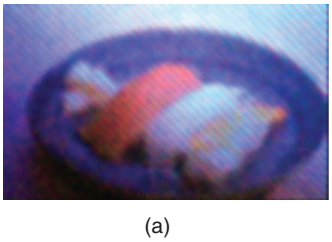

(a)

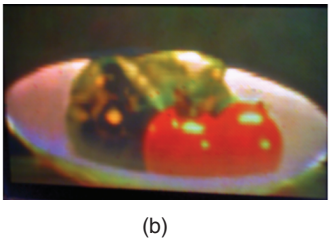

(b)

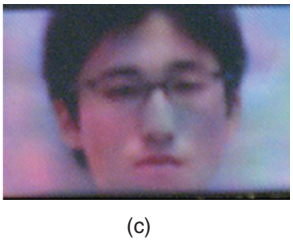

(c)

Figure 13.23 (Plate 23) Reconstructed images from the FP HS recorded from the captured light-field data. (a) Sushi, (b) vegetables, and (c) human face. *See plate section for the color version*

The light-field data captured by the proposed FP 3D image scanner were also employed for the hologram printer explained in Section 13.4. The light-ray data on the RS plane were directly printed as HS by the hologram printer. Examples of reconstructed images are shown in Fig. 13.23 (Plate 23). Holographic images of food, vegetables, and human portraits are reproduced with proper surface reflection characteristics.

13.8 Conclusion and Future Issues

In this chapter, the features of light-field displays and wavefront displays are discussed and the technique for converting ray-based and wavefront-based 3D data is introduced. The limitation of ray-based 3D display is clarified: the resolution of a 3D image becomes lower for images far from the display plane. Thus the important feature of a holographic display is the capability to reproduce deep 3D scenes at high resolution. To take the advantage of holography, a new method is proposed for the computation of hologram using the RS plane.

The proposed method exploits the conversion between the light rays and wavefront, and it becomes possible to employ the advanced rendering techniques in the computation of holograms. It also enables improved occlusion processing and surface shading for the display of deep 3D images at high resolution. Moreover, a system for capturing high-density light-field information is presented. The scanning vertical camera array technique proposed here allows for a small-scale system, controlled by a single PC, collecting high-resolution FP 3D images. The angular-dependent characteristics of 3D objects, that is, specular or glossy surfaces, can be reproduced from captured images owing to the application of the IBR technique and high-resolution parallax data, especially in horizontal direction. High-resolution light-field data captured systems are applied to 3D displays by CGH and HS.

The technology of converting light-rays and wavefronts also enables the integration of 3D imaging systems based on stereoscopic, ray-based, light-field, and holographic methods. Realization of extremely high-quality and innovative holographic display is expected, along with the advancement in device technologies, as well as a system for light-field 3D imaging by integrating ray- and wavefront-based 3D information.

Acknowledgments

This work was partly supported by the JSPS Grant-in-Aid for Scientific Research #17300032, and Toppan Printing Co. The authors acknowledge Hiroaki Yamashita, Takeru Utsugi, Mamoru Inaniwa, in Tokyo Institute of Technology, and Shingo Maruyama, Toppan Printing Co., for providing experimental data.

References

[1] Leith, E.N. and Upatnieks, J., "Wavefront reconstruction with diffused illumination and three-dimensional objects," *J. Opt. Soc. Am.* Vol. **54**, 1295–1301 (1964).

[2] Bjelkhagen, H.I. and Mirlis, E., "Color holography to produce highly realistic three-dimensional images," *Appl. Opt.* Vol. **47**, No. 4, A123–A133 (2008).

[3] St-Hilaire, P., Benton, S. A., Lucente, M. E., Jepsen, M. L., Kollin, J., Yoshikawa, H., and Underkoffler, J. S., "Electronic display system for computational holography," *Proc. SPIE* **1212**, 174 (1990).
[4] Levoy, M. and Hanrahan, P., "Light field rendering," *Computer Graphics (Proc. SIGGRAPH'96)*, 31–42 (1996).
[5] Jones, A., McDowall, I., Yamada, H., Bolas, M., and Debevec, P., "Rendering for an interactive 360° light field display," *ACM Transactions on Graphics* Vol. **26**, No. 3, *Proc. ACM SIGGRAPH 2007*, Article No. 40 (2007).
[6] Wetzstein, G., Lanman, D., Hirsch, M., Heidrich, W., and Raskar, R., "Compressive Light Field Displays," *IEEE Computer Graphics and Applications*, Vol. **32**, No. 5, 6–11 (2012).
[7] Yamaguchi, M., Ohyama, N., and Honda, T., "Holographic 3-D printer," *Proc. SPIE*, Vol. **1212**, 84–90 (1990).
[8] Yamaguchi, M., Ohyama, N., and Honda, T., "Imaging characteristics of holographic stereogram," *Japanese J. of Optics*, (Kogaku), Vol. **22**, No. 11, 714–720 (1993) (in Japanese).
[9] Yamaguchi, M., Hoshino, H., Honda, T., and Ohyama, N., "Phase added stereogram: calculation of hologram using computer graphics technique," *Proc. SPIE*, Vol. **1914**, 25–31 (1993).
[10] Yamaguchi, M., "Ray-based and wavefront-based holographic displays for high-density light-field reproduction," *Proc. SPIE*, Vol. **8043**, 804306 (2011).
[11] Wakunami, K. and Yamaguchi, M., "Calculation for computer generated hologram using ray-sampling plane," *Opt. Express*, Vol. **19**, No. 10, 9086–9101 (2011).
[12] Halle, M., Benton, S. A., Klug, M. A., and Underkoffler, J., "The Ultragram: A generalized holographic stereogram," *Proc. SPIE*, Vol. **1461**, 142–155 (1991).
[13] Yamaguchi, M., Ohyama, N., and Honda, T., "Holographic three-dimensional printer: new method," *Appl. Opt.* Vol. **31**, 217–222 (1992).
[14] Spierings, W. C. and Nuland, E. van, "Development of an office holoprinter II", *Proc. SPIE* Vol. **1667**, 52 (1992).
[15] Bains, S., "The rise and rise of the holographic printer," *OE Reports, SPIE*, May (1996).
[16] Shirakura, A., Kihara, N., and Baba, S., "Instant Holographic Portrait Printing System," *Proc. SPIE*, Vol. **3293** (1998).
[17] Klug, M. A., Klein, A., Plesniak, W. J., Kropp, A. B., and Chen, B., "Optics for full-parallax holographic stereograms," *Proc. SPIE*, Vol. **3011**, 78–88 (1997).
[18] Maruyama, S., Ono, Y., and Yamaguchi, M., "High-density recording of full- color full-parallax holographic stereogram," *Proc. of SPIE*, Vol. **6912**, 69120N-1-10 (2008).
[19] Yamaguchi, M., Endoh, H., Honda, T., and Ohyama, N., "High-quality recording of a full-parallax holographic stereogram with a digital diffuser," *Opt. Lett.* Vol. **19**, No. 2, 135–137 (1994).
[20] Utsugi, T. and Yamaguchi M., "Reduction of the recorded speckle noise in holographic 3D printer," *Opt. Express*, Vol. **21**, No. 1, 662–674 (2013).
[21] Waters, J. P., "Holographic image synthesis utilizing theoretical methods," *Appl. Phys. Lett.* Vol. **9**, 405–407 (1966).
[22] Matsushima, K. and Nakahara, S., "Extremely high-definition full-parallax computer-generated hologram created by the polygon-based method," *Appl. Opt.* Vol. **48**, H54–H63 (2009).
[23] Yatagai, T., "Stereoscopic approach to 3-D display using computer-generated holograms," *Appl. Opt.* Vol. **15**, 2722–2729 (1976).
[24] Underkoffler, J. S., "Occlusion processing and smooth surface shading for fully computed synthetic holography," *Proc. SPIE*, Vol. **3011**, 53–60 (1997).
[25] Matsushima, K., "Exact hidden-surface removal in digitally synthetic full-parallax holograms," *Proc. SPIE*, Vol. **5742**, 25–32 (2005).
[26] Wakunami, K., Yamashita, H., and Yamaguchi, M., "Occlusion culling for computer generated hologram based on ray-wavefront conversion," Submitted to *Optics Express* Vol. **21**, No. 19, 21811–21822 (2013).

[27] Wilburn, B., Joshi, N., Vaish, V., Talvala, E.-V., Antunez, E., Barth, A., *et al*., "High performance imaging using large camera arrays," *ACM Trans. Graphics*, Vol. **24**, No. 3, 765–776 (2005).

[28] Brewin, M., Forman, M., and Davies, N. A., "Electronic capture and display of full-parallax 3D images," *Proc. SPIE*, Vol. **2409**, 118–124 (1995).

[29] Yamaguchi, M., Kojima, R., and Ono, Y., "Full-parallax 3D image scanning for holoprinter," *Nicograph International* (2008).

[30] Zhang, L., "Stereoscopic image generation based on depth images for 3D TV," *IEEE Trans. Broadcasting*, Vol. **51**, No. 2, 191–199 (2005).